Science and Technology Indonesia
e-ISSN:2580-4391 *p*-ISSN:2580-4405
Vol. 10, No. 2, April 2025

Research Paper

Molten Salt Synthesis of $SrTi_{0.95}Fe_{0.05}O_3$: The Effect of Chloride Salt Type Study

Ulvi Dwi Pertiwi[1], Nelly Safitri Anwari[1], Widiya Nur Safitri[2], Edi Pramono[3], Anton Prasetyo[1*]

[1]*Department of Chemistry, Faculty of Science and Technology, Universitas Islam Negeri Maulana Malik Ibrahim Malang, Malang, 65144, Indonesia*
[2]*Department of Chemistry, Faculty of Science and Data Analytics, Institut Teknologi Sepuluh Nopember, Surabaya, 60111, Indonesia*
[3]*Department of Chemistry, Faculty of Mathematics and Natural Science, Universitas Sebelas Maret, Surakarta, 57126, Indonesia*
***Corresponding author**: anton@kim.uin-malang.ac.id

Abstract
Strontium titanate ($SrTiO_3$) refers to a perovskite structure compound reported to have photocatalyst properties. It is well-known that modifying the particle morphology is found to be capable of enhancing the photocatalytic activity as it can increase the reaction sites on the solid surface. Molten salt synthesis is one of the compound synthesis methods to produce the homogeneous particle size as well as the unique morphology. One of the parameters determining the product compound obtained using the molten salt method is the type of salt used. In this study, the $SrTi_{0.95}Fe_{0.05}O_3$ was synthesized by the molten salt method using NaCl, KCl, and NaCl/KCl salt. It also studied the effects of chloride salt type to structure, vibration mode, morphology particle, band gap energy and thermal stability of product samples. The diffractograms showed that $SrTi_{0.95}Fe_{0.05}O_3$ were successfully synthesized; however, the sample obtained using molten KCl salt had the impurities of TiO_2, and $SrCO_3$ (residual of precursors) indicating that the KCl flux was insufficient to make a complete reaction. The characteristic of infrared vibration modes of the $SrTiO_3$ compound were found in all samples. The image of scanning electron microscopy showed that all particle morphology was in the quadrate-particle shape, and the $SrTi_{0.95}Fe_{0.05}O_3$-KCl sample had the smallest particles for having the largest surface area. The Kubelka-Munk equation calculation results showed that all samples' band gap energy was approximately at ~3 eV. The DSC curve showed a relatively similar pattern; therefore, the thermal stability properties of all samples were similar.

Keywords
Fe-doped $SrTiO_3$, Molten Salt Method, Chloride Salt Type

Received: 23 July 2024, Accepted: 7 February 2025
https://doi.org/10.26554/sti.2025.10.2.519-527

1. INTRODUCTION

The perovskite structure compound has the general formula of ABO_3 with A-site cation as rare earth, alkali, or alkaline earth element (such as: Sr, Ba, Pb, Ca, La) and B-site cation as a transition metal (such as: Co, Cr, Ti, Zr, Nb, Ta) (Assirey, 2019; Dawa and Sajjadi, 2024). They have many interesting properties i.e. photocatalyst, ferroelectricity, piezoelectricity, and high dielectric constant (Wei et al., 2020). As reported, these compounds possess a number of photocatalytic properties, those are $SrTiO_3$, $CaTiO_3$, $BaTiO_3$, $NaTaO_3$, and $AgTaO_3$ (Kanhere and Chen, 2014; Rizwan et al., 2019).

Strontium titanate ($SrTiO_3$) is a perovskite compound with several advantages such as strong chemical resistance and physical stability, high-temperature resistance, easiness to modify the crystal structure through substitution in A/B cation, and superior optical properties (Tanigawa et al., 2017; Sudrajat et al., 2020). As a photocatalyst compound, $SrTiO_3$ has a band gap energy of 3.24 eV enabling it to be active in the ultraviolet region (Li et al., 2007b). The high band gap energy of $SrTiO_3$ however has disadvantages when applied as a photocatalyst material as it requires high photon energy as the electron excitation source. In addition, this compound, as reported, has a high electron (e^-)-hole (h^+) recombination rate that can make its photocatalytic ability reduced and its photocatalytic activity lowered (Ahmadi et al., 2021). Therefore, a strategy is required to overcome it such as doping with metal/nonmetal and making heterojunction structures (Fan et al., 2020; Lee et al., 2023).

The partial small substitution of A or B cation sites (doping) on $SrTiO_3$ can change the electronic structure, thereby increasing the photocatalytic activity (Mohan and Mao, 2020; Xu et al., 2023). Abdi et al. (2020) synthesized $SrTiO_3$ with doping La at the A cation site and Fe at the B cation site, which made the band gap energy decreased as the doping concentration increased and the photocatalytic activity to degrade methyl orange was better than that of undoped-$SrTiO_3$. One of the metal elements reported to have potential as a dopant is Fe due to its ionic radius being similar to that of Ti^{4+}, which allows

it to easily enter the crystal lattice. Xie et al. (2008) synthesized Fe-doped $SrTiO_3$ and reported that the light absorption shifted to the visible region. Meanwhile, Sood et al. (2015) reported that Fe doping to TiO_2 can inhibit its rate of e^--h^+ recombination.

The morphology and particle size are able to determine the photocatalyst activity (Chen et al., 2019; Utomo et al., 2024). Gao et al. (2018) reported that cubic $SrTiO_3$ had a better ability to degrade anionic dyes compared to polygonal $SrTiO_3$. Gao et al. (2018) reported that the cubic $SrTiO_3$ has a good ability to degrade a mixture of rhodamine blue and methylene blue dyes. Similarly, Rahman et al. (2012)) reported that spherical Cu-doped $SrTiO_3$ nanoparticles have an excellent ability to degrade methylene blue. In other words, both morphology and particle size of $SrTiO_3$ affect the ability of its photocatalytic activity.

The synthesis of $SrTiO_3$ material can be carried out through several methods, including hydrothermal, molten salt, solvothermal, solid state, and sol-gel methods (Shen et al., 2016; Putri et al., 2024). The molten salt method is well-known as a method for synthesizing metal oxide compounds that can control the morphology and particle size. Boltersdorf et al. (2015) suggested that the molten salt synthesis method can make it possible for metal oxide compounds to have good photocatalytic ability. Many researchers reported the perovskite compound synthesis using molten salt method such as $BaTiO_3$, $BaZrO_3$, and $SrTiO_3$ (Xue et al., 2018). Several researchers also reported the molten salt synthesis of $SrTiO_3$ as conducted by Putri et al. (2022), Zhang et al. (2016) and Wei et al. (2020) synthesizing nanocubic $SrTiO_3$. In addition, many researchers also reported the metal doped $SrTiO_3$ using molten salt synthesis (Abreu et al., 2016; Murai et al., 2021). Prasetiyo et al. (2021) successfully synthesized the cubic Fe-doped $SrTiO_3$ via molten salt method using NaCl salt and reported that its particle size was large and agglomeration formed. It indicates that molten salt synthesis is able to provide a good opportunity to gain nanocrystal $SrTiO_3$ compound; therefore, it will be advantageous in photocatalyst application. However, the reported work of molten salt synthesis of metal doped $SrTiO_3$, particularly Fe doped $SrTiO_3$ synthesis is so far still limited.

There are many factors determining the morphology of particles obtained using molten salt synthesis including synthesis temperature, synthesis time, salt type, and mol ratio product and salt (Kimura, 2011). Previous researchers reported the influence of salt types on the morphology of $SrTiO_3$ particles obtained through the molten salt method. Kato et al. (2013) reported the molten salt synthesis of $SrTiO_3$ using different salt including LiCl, NaCl, KCl, and $SrCl_2$ and found that the salt type influenced its morphology and particle size. It indicates that the type of salt can affect the morphology of the particles obtained. In addition, the type of salt selected can affect the purity of the final product. It is widely known that chloride salts are chemically inert; therefore, it can be expected to produce a pure product (Gupta and Mao, 2021). It indicates that the use of chloride salts offers advantages in compound synthesis using the molten salt method. On the other hand, the studies of salt type to the molten salt synthesis of metal-doped $SrTiO_3$ are still limited especially about study on the effects of chloride salt types on the obtained product compounds. Therefore, further investigation is required. In this research, we synthesized Fe doped $SrTiO_3$ ($SrTi_{0.95}Fe_{0.05}O_3$) compound using molten salt method with a variety of salt types i.e. NaCl, KCl, and mixtures and studied the effect of salt type on compound product.

2. EXPERIMENTAL SECTION

2.1 Materials

Strontium carbonate ($SrCO_3$, Sigma-Aldrich, 99% powder), titanium dioxide (TiO_2, Sigma-Aldrich, 99.9% powder), ferric oxide (Fe_2O_3, Sigma-Aldrich, 99.9% powder), natrium chloride (NaCl, Merck, 99.9% powder), kalium chloride (KCl, Merck, 99.9% powder), silver nitrate ($AgNO_3$, Merck, 99.9% Powder), and acetone (C_3H_6O, Merck).

2.2 Synthesis

$SrTi_{0.95}Fe_{0.05}O_3$ was prepared using molten salt method with the mol ratio of product and salt is 1:7. The precursor was calculated based upon stoichiometry with the target product of 3 gram. The mixture of precursors and salt was crushed in an agate mortar for 1 hour and added with acetone to make it homogeneous. The sample was then transferred to an alumina crucible and calcined at 830 and 855°C for 6 hours, respectively. Then, to remove residual salt the obtained result was washed with hot distilled water. The identification of salt residue in the sample was carried out by testing the washed filtrate using $AgNO_3$ solution. Finally, the cleaned sample was dried in the oven at 90°C for 3 hours.

2.3 Characterization

In this study, the instrumentations used are presented as follows: (a) X-ray diffraction (Rigaku Miniflex diffractometer, Japan) technique was carried out in the range of 2θ= 3-90° with Cu Kα radiation source (λ = 1.54 Å). The obtained diffractogram of the compound was then compared with the $SrTiO_3$ standard, Inorganic Crystal Structure Database (ICSD) No. 80874, and refined using the Le Bail method on Rietica software. (b) Infrared (IR) vibration modes of the sample were determined using Fourier Transform-IR Spectrometer (Bruker Alpha II, USA), (c) The morphology particle and elemental composition of the sample was identified using the scanning electron microscopy-energy dispersive spectroscopy (SEM-EDS) (Jeol JSM-6510, Japan). The morphology and particle size were analyzed using the Image-J software. (d) The surface area of samples were determined using Surface Area Analyzer (Quantachrome Novatouch Lx. Germany). (e) The light absorption property was identified from diffuse reflectance spectroscopy-ultraviolet visible (DRS UV-vis, Thermo Scientific Evolution 220 spectrometer, USA) using the wavelength range of 200-800 nm. The spectrum data were processed by means of the Kubelka-Munk equation to obtain the band gap energy. Here, the Kubelka-Munk calculation used indirect band gap following

the calculation report by Abdi et al. (2020), (f) The thermal analysis was conducted by Differential Scanning Calorimetry (DSC) (Rigaku Thermoplus Evo 2, Japan) at the temperature ranging from 50 to 450°C.

3. RESULTS AND DISCUSSION

Figure 1 shows the diffractograms of $SrTi_{0.95}Fe_{0.05}O_3$ and it can be seen that the diffraction peaks of the synthesized compounds matched with the standard data (ICSD $SrTiO_3$ standard data No. 80874), indicating that the target compounds have been successfully synthesized. The typical peaks of $SrTi_{0.95}Fe_{0.05}O_3$ compounds were found at $2\theta(°)$ = 23; 32.43; 40; 46.62; 52.4; 57.94; 67.92; 72.76, and 77.42. However, the impurities of TiO_2 (2θ (°) = 25.3) and $SrCO_3$ (2θ (°) = 25.8, and 41.5) was still found in the synthesis product using KCl salt, indicating that the reaction was incomplete. In the molten salt synthesis, the process of forming Fe-doped $SrTiO_3$ compounds goes through several mechanisms: dissolution, diffusion, and precursors reacting with each other in molten salt (Li et al., 2007a; Liu et al., 2009). At the diffusion

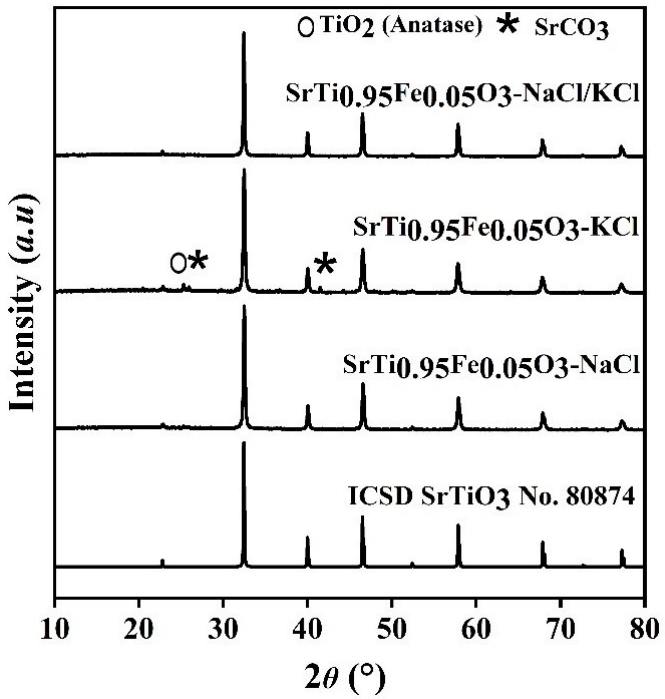

Figure 1. The Diffractograms of $SrTi_{0.95}Fe_{0.05}O_3$ Compounds Synthesized Using the Different Types of Chloride Salt

stage, the reactions of precursors formed product; therefore, the remaining precursors (TiO_2, and $SrCO_3$) as impurities indicated the incomplete reaction. Figure 1 also shows that the diffraction peaks of all samples were high and sharp, which indicated that the salt type did not affect the sample's crystallinity. The Fe-doping in $SrTiO_3$ compounds caused the shift of diffraction peak at $2\theta(°)$ = 32.43 towards a larger position (Figure 2) related to the lattice size change as a result of replacing a small partially of Ti^{4+} (ionic radii (r) = 0.605 Å) metal by Fe^{3+} (r= 0.585 Å) (Abbas and Jamil, 2016; Fuentes et al., 2015).

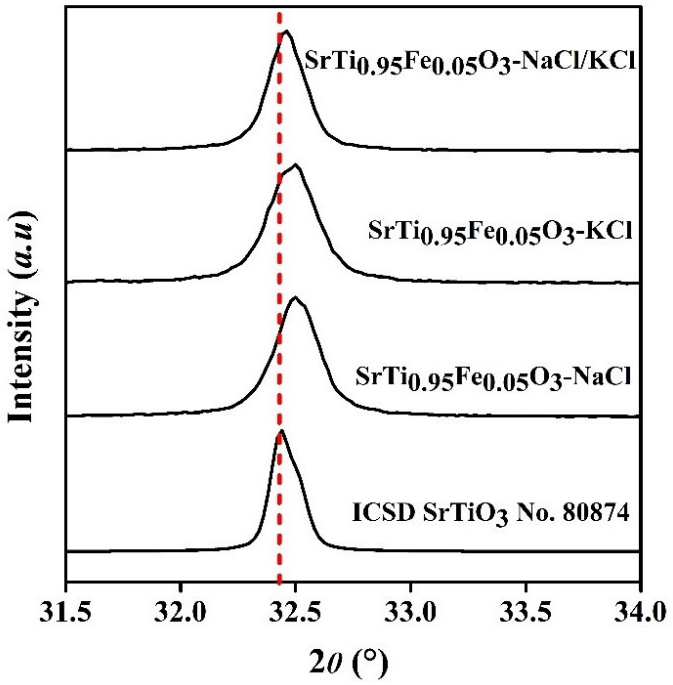

Figure 2. The X-ray Diffraction Peaks Shifting at An Angle of 2θ (°) = 32.43 of $SrTi_{0.95}Fe_{0.05}O_3$ Compounds Synthesized using Different Type of Chloride Salt

The diffractograms of compounds synthesized using NaCl and NaCl/KCl salt were refined by means of Rietica software with the Le-Bail method. The refinement process used the standard of $SrTiO_3$ data on ICSD No. 80874, and the plots of the refinement are shown in Figure 3. The results as summarized in Table 1 shows that the profile residual (Rp) and profile weighted residues (Rwp) values were lower than 15 that indicated the sample diffractograms had good agreement with the standard (Toby, 2006; Nunocha et al., 2022).

Figure 4 shows the IR spectra of the samples in which all of these samples had similar vibrational peaks, i.e. (a) 3200 cm^{-1} relating to OH stretching vibration, (b) 1600 cm^{-1} relating to Ti−O stretching vibration, (c) 1400 cm^{-1} relating to Sr−Ti−O stretching vibration, and (d) 620 cm^{-1} relating to Sr−Ti stretching vibration (Rajkoomar et al., 2020). The OH vibration in all samples indicated the ability of all samples to absorb water. The ability of perovskite to absorb water has been widely reported by previous researchers (Evarestov et al., 2007). A weak vibration peak in sample $SrTi_{0.95}Fe_{0.05}O_3$−KCl was found at 1700 cm^{-1} and corresponded to the vibration of CO_3^{2-} and related to an impurity in sample $SrTi_{0.95}Fe_{0.05}O_3$-KCl ($SrCO_3$) (Zheng et al., 2019).

Figure 5 shows the morphologies and particle size distri-

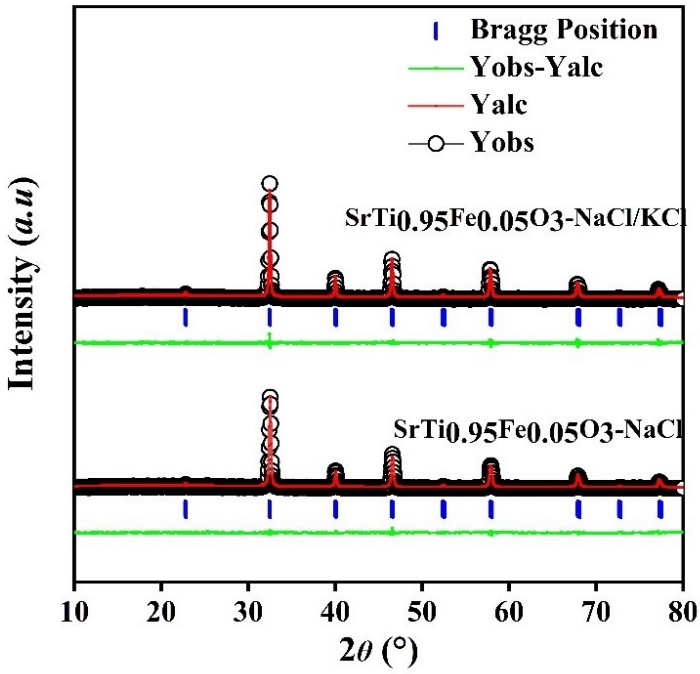

Figure 3. Plots of The Refinement Process Result Using the Le Bail Method for $SrTi_{0.8}Fe_{0.05}O_3$ Compounds Resulting From the Synthesis of NaCl and NaCl/KCl salts

Table 1. The Crystallographic Data of $SrTi_{0.95}Fe_{0.05}O_3$ Synthesized with NaCl and NaCl/KCl Salts Obtained by Refinement Process with Le Bail Method

Parameters	NaCl	NaCl-KCl
Crystal system	Cubic	Cubic
Space group	P*m3m*	*Pm3m*
Asymmetric unit (Z)	1	1
a=b=c (Å)	3.9009 (2)	3.9009 (5)
α, β, γ (°)	90, 90, 90	90, 90, 90
Cell volume (Å3)	59.362 (6)	59.363 (1)
R*p* (%)	8.93	9.13
R*wp* (%)	5.70	6.37
G*oF* (X^2)	0.724	1.090

Table 2. Particle Size Average of Products

Compound	Particle Size Average (μm)
$SrTi_{0.95}Fe_{0.05}O_3$-NaCl	0.2196
$SrTi_{0.95}Fe_{0.05}O_3$-KCl	0.2152
$SrTi_{0.95}Fe_{0.05}O_3$-NaCl/KCl	0.2557

butions of $SrTiO_3$ and Table 2 presents the summary of the calculation results of particle size average. The particle morphology is quadrate-particle shape similar to the work reported

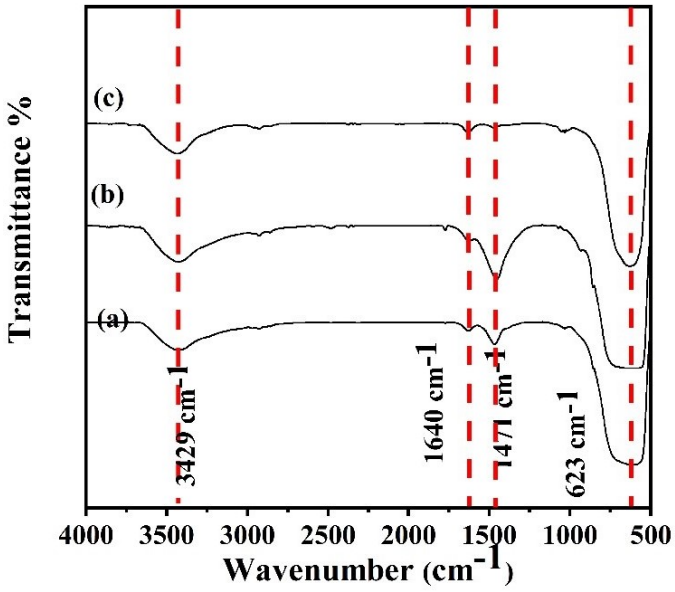

Figure 4. IR Spectra of (a) $SrTi_{0.95}Fe_{0.05}O_3$-NaCl (b) $SrTi_{0.95}Fe_{0.05}O_3$-KCl, (c) $SrTi_{0.95}Fe_{0.05}O_3$-NaCl/KCl

Table 3. Surface Area of Products

Compound	Surface Area (m^2/g)
$SrTi_{0.95}Fe_{0.05}O_3$-NaCl	5.330
$SrTi_{0.95}Fe_{0.05}O_3$-KCl	8.300
$SrTi_{0.95}Fe_{0.05}O_3$-NaCl/KCl	2.466

by Li et al. (2021) that obtained nano quadrate $SrTiO_3$ particles synthesized using NaCl/KCl molten salt method. The SEM images also showed the similar morphology produced from the use of different salt types; this indicated that the chloride salt type did not affect its morphology particle. On the other hand, the study reported by Prasetiyo et al. (2021) obtained the different morphology that gained Fe-doped $SrTiO_3$ in cuboidal-shape using NaCl salt as the flux. This difference was probably related to the differences in synthesis temperature in which the work by Prasetiyo et al. (2021) used a higher temperature (900°C) leading to the maximum particle growth.

The results of average particle size (Table 2) showed that the obtained particle size was relatively small as well as similar to 0.2196-0.2557 μm. It indicated that the nucleation rate was higher than the growth rate of the particles so that a large number of particles were obtained but with a small size. The particle size of sample synthesized using NaCl/KCl salt was found larger than others. It was in view of the lowest melting point of NaCl/KCl (657°C) making the particle growth occurred earlier and leading to the larger particle growth. Besides, the physical properties of salt such as melting point, viscosity, and solubility can affect the morphology and particle size (Liu et al., 2020). At this point, the melting point of salt affects

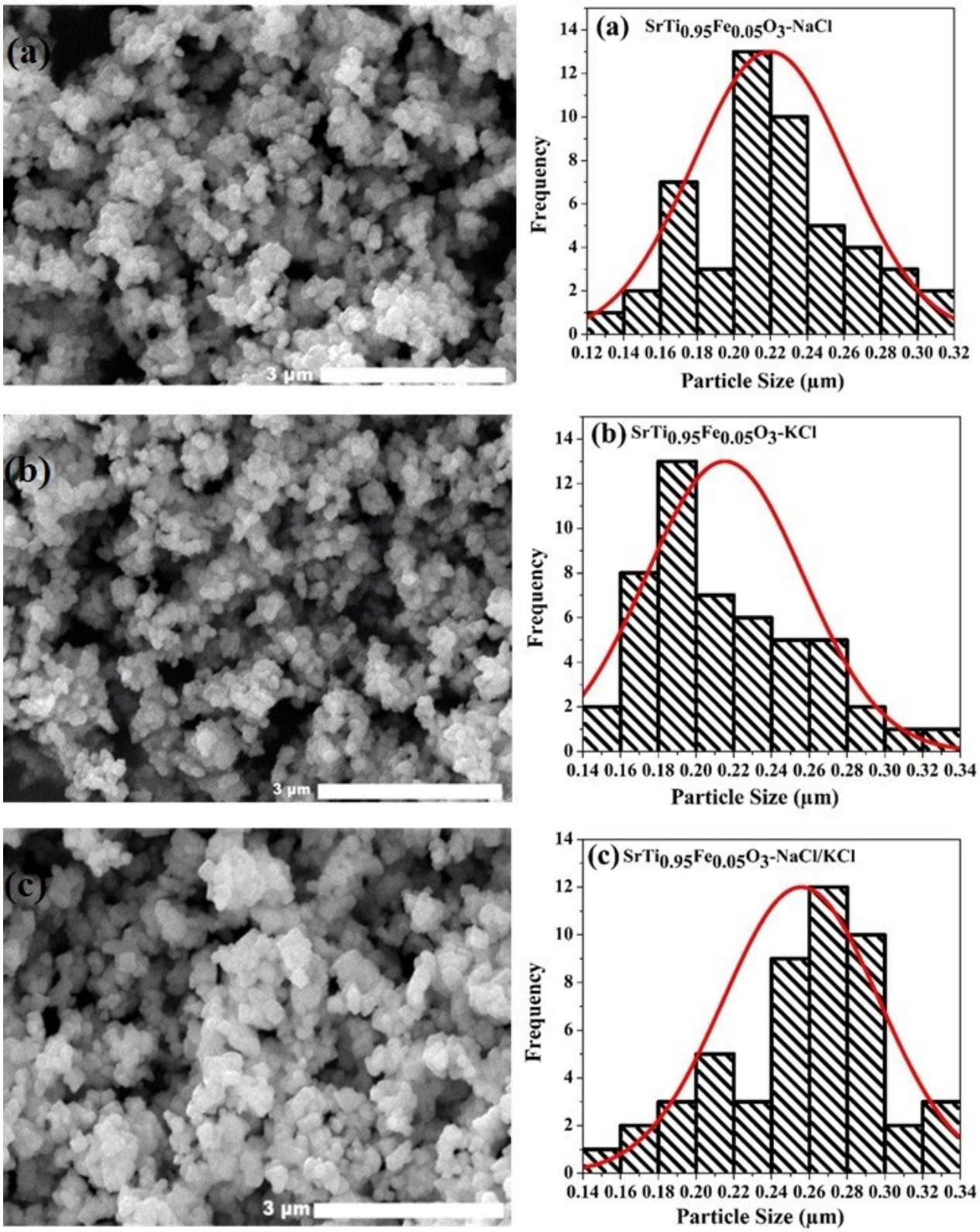

Figure 5. SEM Images and Particle Size Distributions of $SrTi_{0.95}Fe_{0.05}O_3$ Synthesized using (a) NaCl, (b) KCl, and (c) NaCl/KCl Salt

Table 4. The Percentage of Element Mass in $SrTi_{0.95}Fe_{0.05}O_3$

Element	$SrTi_{0.95}Fe_{0.05}O_3$-NaCl (% mass)	$SSrTi_{0.95}Fe_{0.05}O_3$-KCl (% mass)	$SrTi_{0.95}Fe_{0.05}O_3$-NaCl/KCl (% mass)
Stronsium (Sr)	41.00	38.47	41.71
Titanium (Ti)	29.59	27.64	29.49
Iron (Fe)	3.62	3.71	3.44
Oxygen (O)	25.79	30.18	25.36

the formation of particles. The faster the melting point of salt, the quicker the formation of crystal seeds (nucleation stage) (Kimura, 2011). In addition, the viscosity of the salt affects the formation of particles. It corresponds to the lower viscosity induces faster diffusion rate of anions and cations precursors (Li et al., 2007b). Wakao et al. (1991) reported that NaCl and KCl had almost the same viscosity at the same temperature. Therefore, it is possible to obtain the relatively similar morphology and particle size. Table 3 presents the summary of the results of the surface area calculations for the samples in which it can be seen that sample $SrTi_{0.95}Fe_{0.05}O_3$-KCl had the largest surface area. It corresponds to the particle size distribution data that sample $SrTi_{0.95}Fe_{0.05}O_3$-KCl has the smallest particle size (Bullard et al., 2021). Meanwhile, the EDS spectra results (Table 4) showed that the elements contained in $SrTi_{0.95}Fe_{0.05}O_3$ were strontium, titanium, iron, and oxygen indicating that the samples were successfully doped by Fe.

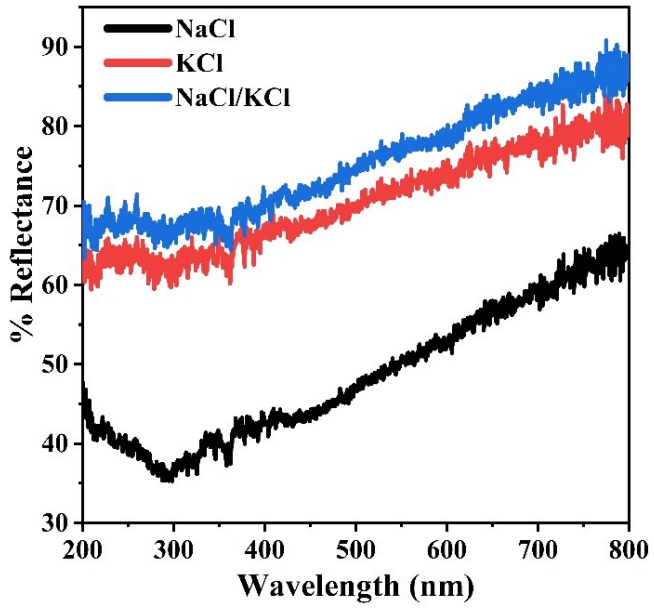

Figure 6. The Percentage of Reflectance Value Vs. The Wavelength of DRS Spectra of $SrTi_{0.95}Fe_{0.05}O_3$ Compounds

Figure 6 shows the reflectance spectra of $SrTi_{0.95}Fe_{0.05}O_3$ and it can be seen that the percentage of reflectance of the sample synthesized using NaCl salt was found less than others, which also showed their higher percentage of absorbance. The difference of percentage of reflectance was probably due to the agglomeration or aggregation particle determining the optical absorption (Melcher et al., 2017). The SEM images (Figure 5) showed that the agglomeration was found in all samples. The Kubelka-Munk equation processed the percentage of reflectance to obtain the band gap energy value. Figures 7 shows the Tauc Plots of $SrTi_{0.95}Fe_{0.05}O_3$ and Table 5 depicts the results of band gap energy calculations. The results of calculation showed that all samples had the relatively similar band gap energy values. The band gap energy of $SrTi_{0.95}Fe_{0.05}O_3$ compound had a lower value compared to the pure $SrTiO_3$ compound (3.24 eV) (Li et al., 2021). It was due to the formation of a new sub band, i.e. d orbital from Fe doping (Abbas and Jamil, 2016). The formation of this new sub band gave the change of the electronic transition from O-2*p* (VB) to Ti-*d* (CB) becomes O-2*p* (VB) to Fe/Ti−*d* (CB), narrowing the band gap energy (Shafique et al., 2021).

Table 5. The Band Gap Energies and Wavelength Absorptions of $SrTi_{0.95}Fe_{0.05}O_3$

Compound	Band Gap Energy (eV)	Wavelength (nm)
$SrTi_{0.95}Fe_{0.05}O_3$-NaCl	3.01	412
$SrTi_{0.95}Fe_{0.05}O_3$-KCl	3.00	413
$SrTi_{0.95}Fe_{0.05}O_3$-NaCl/KCl	2.97	417

Figure 8 shows the thermogram DSC curve of samples and it can be seen that all samples had the similar pattern and no exothermic or endothermic changes were observed. It indicated that all samples had the similar thermal stability trend at the temperature ranging from 50-450°C. The DSC curve also showed that there was no phase transition at 50-450°C. The phase transition of $SrTiO_3$ was not detected due to the short measurement temperature range, while the transition phase occurred outside of this range. $SrTiO_3$ was reported to have a phase transition temperature (structural change from cubic with space group P*m3m* to tetragonal with space group P*4mm*) at 105 K (-168.15°C) and melts at 2080°C (Phoon et al., 2019).

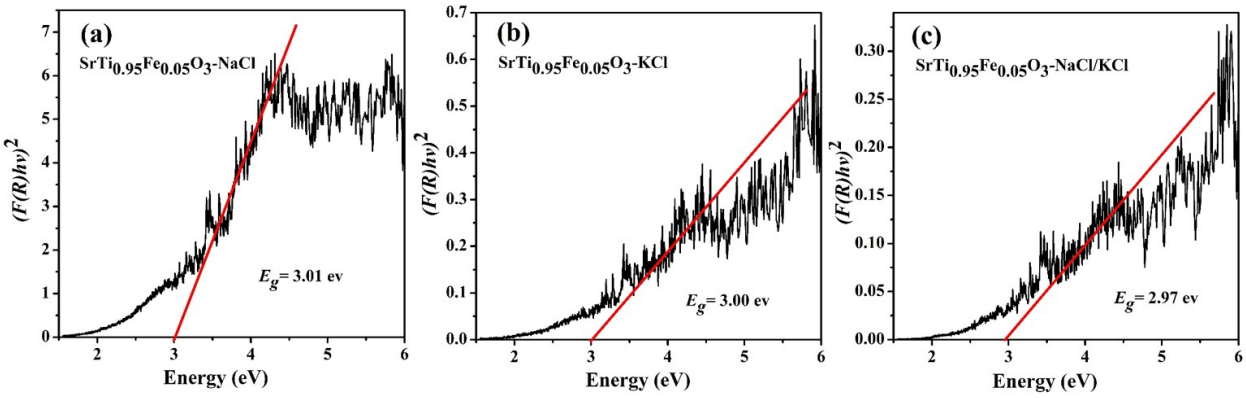

Figure 7. The Tauc Plots of $SrTi_{0.95}Fe_{0.05}O_3$ Synthesized using (a) NaCl (b) KCl, and (c) NaCl/KCl Salts

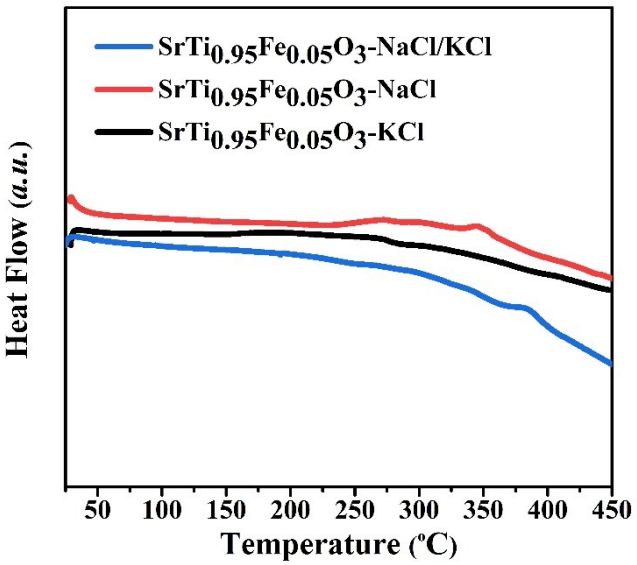

Figure 8. DSC Curve of Samples

4. CONCLUSIONS

The $SrTi_{0.95}Fe_{0.05}O_3$ compounds have been successfully synthesized using the molten salt method with the salt types of NaCl, KCl, and NaCl/KCl. However, the impurities compounds (TiO_2 and $SrCO_3$) were still found in sample $SrTi_{0.95}Fe_{0.05}O_3$−KCl, which indicated that the KCl salt melt has not been able to fully facilitate the reaction of the precursors. The IR spectra of all samples showed the characteristic vibrations of the $SrTiO_3$ compound observed at a peak at the wavenumber 1400 cm^{-1}, which related to Sr−Ti−O stretching vibration, and at a wavenumber of 620 cm^{-1}, which related to Sr−Ti stretching vibration. The obtained morphology was a quadrate-shape with relatively similar particle size. It indicated that the particle growth mechanism of $SrTi_{0.95}Fe_{0.05}O_3$ was similar for all types of chloride salts used. All samples had the relatively similar band gap energy (~3.00 eV/~413 nm) and lower than undoped related to the new formation electronic transition due to Fe dopant. The obtained band gap energy values indicate that this compound offers advantages for photocatalyst applications as it can operate in the visible light spectrum (purple color). Meanwhile, the thermal analysis showed that all samples were similar in thermal stability. The research results indicated that the molten salt method (using NaCl and NaCl/KCl salts) can be used to synthesize Fe-doped $SrTiO_3$ compounds with high purity and uniform small particle size.

5. ACKNOWLEDGEMENT

We thank the Department of Chemistry, Faculty of Science and Technology, Universitas Islam Negeri Maulana Malik Ibrahim Malang for the laboratory facilities for us.

REFERENCES

Abbas, H. A. and T. S. Jamil (2016). Nano sized Fe Doped Strontium Titanate for Photocatalytic Degradation of Dibutyl Phthalate Under Visible Light. *Advanced Materials Letters*, **7**(6); 467–471

Abdi, M., V. Mahdikhah, and S. Sheibani (2020). Visible Light Photocatalytic Performance of La-Fe Co-Doped SrTiO3 Perovskite Powder. *Optical Materials*, **102**; 109803

Abreu, Y. G., J. C. Soares, R. L. Moreira, and A. Dias (2016). Monitoring the Structural and Vibrational Properties in RE-Doped SrTiO3 Ceramic Powders. *The Journal of Physical Chemistry C*, **120**(30); 16960–16968

Ahmadi, M., M. S. S. Dorraji, I. Hajimiri, and M. H. Rasoulifard (2021). The Main Role of CuO Loading Against Electron-Hole Recombination of SrTiO3: Improvement and Investigation of Photocatalytic Activity, Modeling, and Optimization by Response Surface Methodology. *Journal of Photochemistry and Photobiology A: Chemistry*, **404**; 112886

Assirey, E. A. R. (2019). Perovskite Synthesis, Properties and Their Related Biochemical and Industrial Application. *Saudi Pharmaceutical Journal*, **27**(6); 817–829

Boltersdorf, J., N. King, and P. A. Maggard (2015). Flux-Mediated Crystal Growth of Metal Oxides: Synthetic Tunability of Particle Morphologies, Sizes, and Surface Features for Photocatalysis Research. *CrystEngComm*, **17**; 2225–2241

Bullard, J. W., Q. Jin, and K. A. Snyder (2021). How Do Specific Surface Area and Particle Size Distribution Change When Granular Media Dissolve? *Chemical Engineering Journal*, **406**; 127098

Chen, K., Q. Fan, C. Chen, Z. Chen, A. Alsaedi, and T. Hayat (2019). Insights into the Crystal Size and Morphology of Photocatalysts. *Journal of Colloid and Interface Science*, **538**; 638–647

Dawa, T. and B. Sajjadi (2024). Exploring the Potential of Perovskite Structures for Chemical Looping Technology: A State-of-the-Art Review. *Fuel Processing Technology*, **253**; 108022

Evarestov, R. A., A. V. Bandura, and E. N. Blokhin (2007). The Water Adsorption on the Surfaces of SrMO3 (M = Ti, Zr, and Hf) Crystalline Oxides: Quantum and Classical Modelling. *Journal of Physics: Conference Series*, **93**; 012001

Fan, Y., Y. Liu, H. Cui, W. Wang, Q. Shang, X. Shi, G. Cui, and B. Tang (2020). Photocatalytic Overall Water Splitting by SrTiO3 with Surface Oxygen Vacancies. *Nanomaterials*, **10**(12); 1–10

Fuentes, S., P. Muñoz, N. Barraza, E. Chávez-Ángel, and C. M. S. Torres (2015). Structural Characterisation of Slightly Fe-Doped SrTiO3 Grown via a Sol–Gel Hydrothermal Synthesis. *Journal of Sol-Gel Science and Technology*, **75**(3); 593–601

Gao, H., H. Yang, and S. Wang (2018). Hydrothermal Synthesis, Growth Mechanism, Optical Properties and Photocatalytic Activity of Cubic SrTiO3 Particles for the Degradation of Cationic and Anionic Dyes. *Optik*, **175**; 237–249

Gupta, S. K. and Y. Mao (2021). A Review on Molten Salt Synthesis of Metal Oxide Nanomaterials: Status, Opportunity, and Challenge. *Progress in Materials Science*, **117**; 100734

Kanhere, P. and Z. Chen (2014). A Review on Visible Light Active Perovskite-Based Photocatalysts. *Molecules*, **19**(12); 19995–20022

Kato, H., M. Kobayashi, M. Hara, and M. Kakihana (2013). Fabrication of SrTiO3 Exposing Characteristic Facets Using Molten Salt Flux and Improvement of Photocatalytic Activity for Water Splitting. *Catalysis Science & Technology*, **3**(7); 1733–1738

Kimura, T. (2011). *Molten Salt Synthesis of Ceramic Powders*. IntechOpen, London, UK

Lee, D. E., M. K. Kim, M. Danish, and W. K. Jo (2023). State of the Art Review on Photocatalysis for Efficient Wastewater Treatment: Attractive Approach in Photocatalyst Design and Parameters Affecting the Photocatalytic Degradation. *Catalysis Communications*, **183**; 106764

Li, J., X. Tang, Q. Liu, Y. Jiang, and Z. Tang (2021). Resistive Switching and Optical Properties of Strontium Ferrate Titanate Thin Film Prepared via Chemical Solution Deposition. *Journal of Advanced Ceramics*, **10**(5); 1001–1010

Li, Z., S. Zhang, and W. E. Lee (2007a). Molten Salt Synthesis of Zinc Aluminate Powder. *Journal of the European Ceramic Society*, **27**(12); 3407–3412

Li, Z., X. Zhang, J. Hou, and K. Zhou (2007b). Molten Salt Synthesis of Anisometric Sr3Ti2O7 Particles. *Journal of Crystal Growth*, **305**(1); 265–270

Liu, D., Q. Fu, and Y. Chu (2020). Molten Salt Synthesis, Formation Mechanism, and Oxidation Behavior of Nanocrystalline HfB2 Powders. *Journal of Advanced Ceramics*, **9**; 35–44

Liu, Y. F., Y. N. Lu, M. Xu, L. F. Zhou, and S. Z. Shi (2009). Topochemical Reaction of SrTiO3 Platelet Crystals Based on Sr3Ti2O7 Platelet Precursor in Molten Salt Synthesis Process. *Materials Chemistry and Physics*, **114**(1); 37–42

Melcher, J., N. Barth, C. Schilde, A. Kwade, and D. Bahnemann (2017). Influence of TiO2 Agglomerate and Aggregate Sizes on Photocatalytic Activity. *Journal of Materials Science*, **52**; 1047–1056

Mohan, S. and Y. Mao (2020). Molten Salt Synthesized Submicron Perovskite La1–xSrxCoO3 Particles as Efficient Electrocatalyst for Water Electrolysis. *Frontiers in Materials*, **7**; 1–10

Murai, K. I., T. Nishiura, R. Nagata, and T. Moriga (2021). Fabrication and Evaluation of Ca-Doped SrTiO3 Thermoelectric Materials by Molten Salt Method. *International Journal of Modern Physics B*, **35**(14-16)

Nunocha, P., M. Kaewpanha, T. Bongkarn, A. Eiad-Ua, and T. Suriwong (2022). Effect of Nb Doping on the Structural, Optical, and Photocatalytic Properties of SrTiO3 Nanopowder Synthesized by Sol-Gel Auto Combustion Technique. *Journal of Asian Ceramic Societies*, **10**(3); 583–596

Phoon, B. L., C. W. Lai, J. C. Juan, P.-L. Show, and W.-H. Chen (2019). A Review of Synthesis and Morphology of SrTiO3 for Energy and Other Applications. *International Journal of Energy Research*, **43**; 5151–5174

Prasetiyo, A. D., D. R. Novianti, H. Maulidianingtiyas, and A. Prasetyo (2021). Molten Salt Synthesis of Photocatalyst Material SrTix-1FexO3 (x= 0, 0.05, 0.1, 0.15, and 0.2). In *AIP Conference Proceedings*, volume 2349. page 020036

Putri, Y. E., T. P. Wendari, D. Dinda, M. Arnel, H. Faradilla, R. Refinel, and M. Efdi (2024). The Hydrothermal Synthesis of SrTiO3 Nanopolyhedral with the Assistance of Surfactants and Their Optical Characteristics. *Case Studies in Chemical and Environmental Engineering*, **9**; 100601

Putri, Y. E., T. P. Wendari, A. A. Rahmah, R. Refinel, S. M. Said, N. Sofyan, and D. V. Wellia (2022). Tuning the Morphology of SrTiO3 Nanocubes and Their Enhanced Electrical Conductivity. *Ceramics International*, **48**(4); 5321–5326

Rahman, Q. I., M. Ahmad, S. K. Misra, and M. Lohani (2012). Efficient Degradation of Methylene Blue Dye Over Highly Reactive Cu-Doped Strontium Titanate (SrTiO3) Nanoparticles Photocatalyst Under Visible Light. *Journal of Nanoscience and Nanotechnology*, **12**; 7181–7186

Rajkoomar, N., A. Murugesan, S. Prabu, and R. M. Gengan (2020). Synthesis of Methyl Piperazinyl-Quinolinyl α-Aminophosphonates Derivatives Under Microwave Irra-

diation with Pd–SrTiO3 Catalyst and Their Antibacterial and Antioxidant Activities. *Phosphorus, Sulfur, and Silicon and the Related Elements*, **195**(12); 1031–1038

Rizwan, M., M. Anwar, Z. Usman, M. Shakil, S. S. A. Gillani, H. B. Jin, C. B. Cao, and U. Mushtaq (2019). Implementation of Magnesium Doping in SrTiO3 for Correlating Electronic, Structural and Optical Properties: A DFT Study. *Chinese Journal of Physics*, **62**; 388–394

Shafique, H., S. A. Aldaghfag, M. Kashif, M. Zahid, M. Yaseen, J. Iqbal, A. Misbah, and R. Neffati (2021). Magnetic and Optical Characteristics of Fe-Doped SrTiO3 Perovskite Compound: A First Principle Study. *Chalcogenide Letters*, **18**(10); 589–599

Shen, H., Y. Lu, Y. Wang, Z. Pan, G. Cao, X. Yan, and G. Fang (2016). Low-Temperature Hydrothermal Synthesis of SrTiO3 Nanoparticles Without Alkali and Their Effective Photocatalytic Activity. *Journal of Advanced Ceramics*, **5**; 298–307

Sood, S., A. Umar, S. K. Mehta, and S. K. Kansal (2015). Highly Effective Fe-Doped TiO2 Nanoparticles Photocatalysts for Visible-Light Driven Photocatalytic Degradation of Toxic Organic Compounds. *Journal of Colloid and Interface Science*, **450**; 213–223

Sudrajat, H., M. M. Fadlallah, S. Tao, M. Kitta, N. Ichikuni, and H. Onishi (2020). Dopant Site in Indium-Doped SrTiO3 Photocatalysts. *Physical Chemistry Chemical Physics*, **22**; 19178–19187

Tanigawa, S., T. Takashima, and H. Irie (2017). Enhanced Visible-Light-Sensitive Two-Step Overall Water-Splitting Based on Band Structure Controls of Titanium Dioxide and Strontium Titanate. *Journal of Materials Science and Chemical Engineering*, **5**(1); 129–141

Toby, B. H. (2006). R Factors in Rietveld Analysis: How Good is Good Enough? *Powder Diffraction*, **21**(1); 67–70

Utomo, W. P., P. A. I. Afifah, A. I. Rozafia, A. A. Mahardika, E. Santoso, R. Liu, and D. Hartanto (2024). Modulation of Particle Size and Morphology of Zinc Oxide in Graphitic Carbon Nitride/Zinc Oxide Composites for Enhanced Photocatalytic Degradation of Methylene Blue. *Surfaces and Interfaces*, **46**; 104017

Wakao, M., K. Minami, and A. Nagashima (1991). Viscosity Measurements of Molten LiCl in the Temperature Range 886-1275 K. *International Journal of Thermophysics*, **12**; 223–230

Wei, H., J. Cai, Y. Zhang, X. Zhang, E. A. Baranova, J. Cui, Y. Wang, X. Shu, Y. Qin, J. Liu, and Y. Wu (2020). Synthesis of SrTiO3 Submicron Cubes with Simultaneous and Competitive Photocatalytic Activity for H2O Splitting and CO2 Reduction. *RSC Advances*, **10**; 42619–42627

Xie, T. H., X. Sun, and J. Lin (2008). Enhanced Photocatalytic Degradation of RhB Driven by Visible Light-Induced MMCT of Ti(IV)-O-Fe(II) Formed in Fe-Doped SrTiO3. *Journal of Physical Chemistry C*, **112**(26); 9753–9759

Xu, Y., Y. Liang, Q. He, R. Xu, D. Chen, X. Xu, and H. Hu (2023). Review of Doping SrTiO3 for Photocatalytic Applications. *Bulletin of Materials Science*, **46**(6)

Xue, P., H. Wu, Y. Lu, and X. Zhu (2018). Recent Progress in Molten Salt Synthesis of Low-Dimensional Perovskite Oxide Nanostructures, Structural Characterization, Properties, and Functional Applications: A Review. *Journal of Materials Science and Technology*, **34**(6); 914–930

Zhang, G., W. Jiang, S. Hua, H. Zhao, L. Zhang, and Z. Sun (2016). Constructing Bulk Defective Perovskite SrTiO3 Nanocubes for High Performance Photocatalyst. *Nanoscale*, **8**; 16963–16968

Zheng, K., T. Chen, J. Zhang, X. Tian, H. Ge, T. Qiao, J. Lei, X. Li, T. Duan, and W. Zhu (2019). Nano-Montmorillonite Regulated Crystallization of Hierarchical Strontium Carbonate in a Microbial Mineralization System. *Materials*, **12**; 1392

